4/8/96

SANDIA REPORT

SAND96–0535 • UC–411
Unlimited Release
Printed March 1996

Ion Energy and Angular Distributions in Inductively Coupled Argon RF Discharges

Joseph R. Woodworth, Merle E. Riley, Dorothy C. Meister,
Ben P. Aragon, Minh S. Le, Herbert H. Sawin

Prepared by
Sandia National Laboratories
Albuquerque, New Mexico 87185 and Livermore, California 94550
for the United States Department of Energy
under Contract DE-AC04-94AL85000

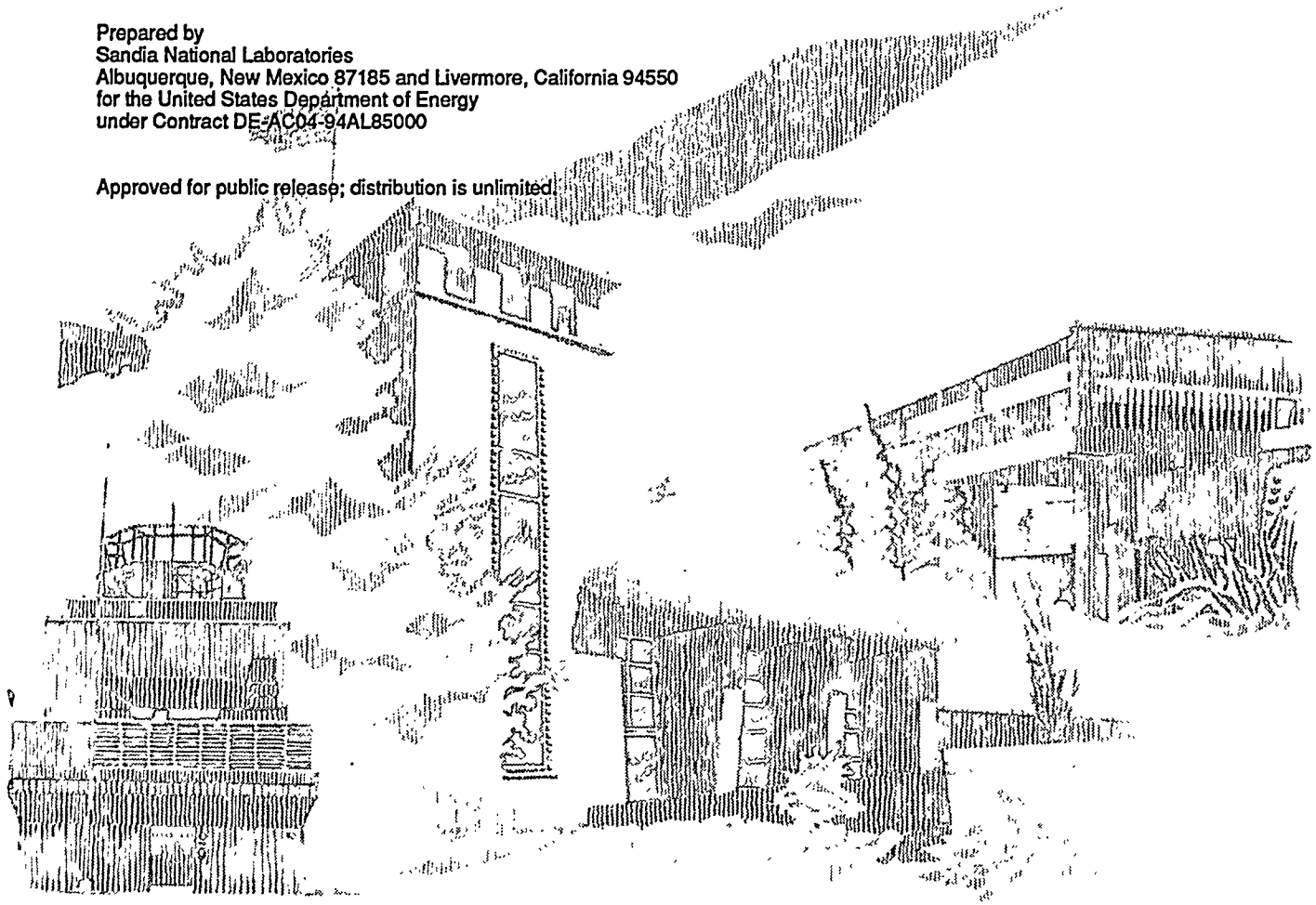

Issued by Sandia National Laboratories, operated for the United States Department of Energy by Sandia Corporation.

Available to DOE and DOE contractors from
Office of Scientific and Technical Information
PO Box 62
Oak Ridge, TN 37831

Prices available from (615) 576-8401, FTS 626-8401

Available to the public from
National Technical Information Service
US Department of Commerce
5285 Port Royal Rd
Springfield, VA 22161

NTIS price codes
Printed copy: A03
Microfiche copy: A01

SAND96 - 0535
Unlimited Release
Printed March 1996

Distribution
Category UC - 411

Ion Energy and Angular Distributions in Inductively Coupled Argon RF Discharges

Joseph R. Woodworth, Merle E. Riley, Dorothy C. Meister, Ben P. Aragon,
Laser, Optics and Remote Sensing Department
Sandia National Laboratories, Albuquerque, NM 87185-1423

Minh S. Le, Herbert H. Sawin, Department of Electrical Engineering, Massachusetts Institute of Technology, Cambridge, Mass. 02139

Abstract

We report measurements of the energies and angular distributions of positive ions in an inductively coupled argon plasma in a GEC reference cell. Use of two separate ion detectors allowed measurement of ion energies and fluxes as a function of position as well as ion angular distributions on the discharge centerline. The inductive drive on our system produced high plasma densities (up to $10^{12}/cm^3$ electron densities) and relatively stable plasma potentials. As a result, ion energy distributions typically consisted of a single feature well separated from zero energy. Mean ion energy was independent of rf power and varied inversely with pressure, decreasing from 29 eV to 12 eV as pressure increased from 2.4 m Torr to 50 mTorr. Half-widths of the ion angular distributions in these experiments varied from 5 degrees to 12.5 degrees, or equivalently, transverse temperatures varied from 0.2 to 0.5 eV with the distributions broadening as either pressure or RF power were increased.

I. Introduction

Plasma discharges are widely used to etch semiconductors, oxides, and metals in the production of very-large-scale integrated circuits. Energetic ions in these discharges play a critical role in the process, influencing the etch rates, etch profiles, and selectivity to different materials. [1,2,3] Several groups are actively engaged in developing computational models of these plasma processing discharges. [4-8] In order to validate the predictions of these models, detailed experimental measurements of plasma praameters are required. In this paper, we report ion fluxes and energy distributions versus radius as well as ion angular distributions measured on the centerline, for inductively coupled discharges in argon.

Gridded "retarding field" energy analyzers have been used to measure ion energy distributions for several decades.[9,10,11] A number of authors have examined the energy distributions using gridded energy analyzers in capacitively coupled[12-17] and inductively coupled [18-21] RF discharges. More recently, gridded energy analyzers have been used to measure ion energies in electron-cyclotron-resonance driven plasmas [22,23] and in plasmas for controlled fusion research.[24,25] In addition to gridded energy analyzers, a number of other electrostatic detectors have been used to measure ion energies. [26-31]

The angular distribution of the ions striking the wafer strongly influences the etch anisotropy, which in turn influences the smallest possible feature size that can be etched on the wafer. Very few measurements have been reported on ion angular distributions in plasma etching discharges.[12, 13] To our knowledge, no angular distribution measurements have been previously reported for the "high-density" inductively coupled rf discharges which are coming into increasing use in the microelectronics industry.

II. Apparatus:

A. GEC Reference Cell

Our experiments were carried out in a Gaseous Electronics Conference Reference Cell[32, 33] which had been modified to produce inductively coupled discharges.[34] The Gaseous Electronics Conference Reference Cell (GEC Ref. Cell) was developed to allow workers at a number of different laboratories to directly compare measurements in a cell which has good diagnostic access and is is similar to plasma reactors used in the semiconductor industry. A schematic of our cell, including the two ion detectors we used, is shown in Fig. 1. The Faraday shield shown in Fig. 1 was only inserted for one set of experiments as discussed in Section III A. The GEC Ref. Cell and the chamber containing the isolated ion detector were evacuated by turbomolecular pumps and had base pressures below 2 x 10^{-7} Torr.

B. Isolated Ion Detector

The first detector was a gridded energy analyzer which was isolated from the plasma by placing it behind a pinhole in the grounded lower electrode, in a separate vacuum system. This detector was used to measure both ion energy spectra and ion angular distributions on the centerline of the discharge. This detector was built at Sandia, based on earlier designs at MIT.[12,13] A schematic of the isolated detector is shown in Fig. 2. The detector contains three screen grids and a series of annular collecting rings. All three grids and the collecting rings form sections of concentric hemispheres which are centered on the pinhole. The three screen grids [35] were pressed over spherical brass mandrels and then tack-welded to stainless steel washers as described by Taylor. [36] The first grid (nearest the pinhole) and the third grid were of 50 lines per inch stainless steel woven screen and were 92% open. The first grid was grounded to provide a field-free drift region between the pinhole and the detector. The third grid was held at a negative voltage (~-10.2 V) to repel discharge electrons and suppress secondary electron emission from the collecting rings. The second grid was made of 100 line-per-inch stainless steel screen which was 81% open. The second grid was scanned in voltage from 0 to + 40 V to sweep out the ion energy spectrum. Only ions with energies greater than the voltage on the second grid were passed by the grids and detected by the collecting rings. Thus, the ion energy spectrum wwas the derivative of the signal at the collecting rings with respect to the voltage on the second grid.

The nine annular collecting rings were formed on a concave semispherical surface machined into a piece of VESPEL™ polyimide. [32] After nine small holes were drilled from the back side to the semispherical side of the polyimide piece, wires were glued through the holes to allow connection to the electrode rings. To form the electrodes, layers of chromium and copper were sputter-deposited over the polyimide and a layer of nickel was plated over the copper. We used a lathe to cut nine narrow (~.01" wide) circular grooves through the conducting films to separate the nine annular electrodes. Each electrode subtended an angle of approximately 4 degrees to a normal through the pinhole.

A variety of pinholes were used in these experiments. The ion energy spectra presented here were taken with a 10-micron-diameter pinhole in a 2.5-micron-thick nickel foil. Unless otherwise noted, the ion angular data presented here were taken using a 2-micron pinhole in a 1.5-micron-thick gold foil [33]. Due to the finite thickness of the pinhole foils, the pinholes looked slightly smaller to ions approaching the pinhole at large angles to the pinhole normal. We corrected for this effect as explained in references 7 and 8. In most cases, the corrections changed the value of the signals by less than 10%.

The data collection system for the isolated detector was controlled by a computer operating on LabVIEW for Windows. Voltages on the second and third grids of the detector were controlled by two Kepco PAT 100-0.2 power supplies which were in turn controlled by a Kepco SN-488 controller. Currents from the collector rings were measured with a HP 6512 electrometer. Data points were collected at 0.25-Volt intervals,

with five measurements at each voltage being averaged to comprise one point. The data was then differentiated to obtain the ion energy distributions.

B. Mini-Ion Detector

The second ion detector was a miniaturized gridded energy analyzer, which operated directly in the discharge, as shown in Fig. 1. This detector, developed at the Massachussetts Institute of Technology [22,23], was extremely small, measuring 0.32 cm by 5 cm. The small size of this detector gave it high energy resolution (sub-eV FWHM[17]) and allowed it to be mounted on a stalk and moved about in the discharge to map out spatial variations in the plasma. Figure 3 shows a schematic of this detector. This detector used only two screen grids. The first grid was grounded and the second grid was held at a negative potential to repel discharge electrons and suppress secondary electron production from the collector. In order to sweep out the ion energy distribution, the nickel-foil collection electrode itself was scanned from 0 to + 50 Volts. Because this detector was immersed in the plasma, the grid size and spacing between grids needed to be very small -- comparable to the ~15 micron Debye lengths seen in the plasma. Hence, 78 line-per-mm grids [39] were used and the grids were separated by 0.25 mm-thick alumina spacers.

In the data collection system for the mini-detector, a computer-controlled operational amplifier circuit (Apex PA08) applied voltage to the collector. Collector current was read by a Hewlett Packard HP-485 floating picoammeter and sent to the computer through an Analog Devices AD-289J isolation amplifier. Data was collected in 0.18-Volt increments and was filtered during the analysis by taking a sliding average over 0.54 Volts.

III. Results and Discussion

A. Ion Energy Distributions

Figure 4 shows raw data and an ion energy distribution obtained with the isolated detector for a 5 millitorr, 300 Watt rf discharge in argon. The raw data is current in Amps/cm^2 as a function of voltage on the second screen of the analyzer. The ion energy distribution is the deravitive of the raw data with respect to voltage. Figures 5 and 6 show ion energy distributions in argon discharges as a function of pressure and power as recorded by the isolated detector. Figure 7 shows energy distributions measured at several different radial locations by the mini-ion detector. Figures 8 and 9 show plots of total ion flux versus pressure and power and mean ion energy vs pressure as measured by the isolated detector.

The most striking thing about these ion energy distributions is their simplicity. They show one relatively narrow feature, well separated from zero energy. This is in contrast to ion energy distributions measured in capacitive discharges[12], which typically show a continuum of ion energies from a high energy limit down to near zero ion energy.

The differences between our ion energy distributions and those seen in capacitive discharges arise from the differences in the plasma potentials, sheath dimensions and pressure ranges between the two cases.[12] In capacitively-coupled discharges, the plasma potential varies from near zero to the full rf potential during each rf cycle. Also, capacitive discharges normally are operated at relatively high pressures (up to 1 torr) and low electron densities ($n_e = 10^9$ to 10^{11} /cm^{-3}) which yields relatively wide, collisional sheaths. Therefore, the energies of the ions at the electrode in capacitive discharges can vary greatly, depending on the phase of the rf cycle when they start across the sheath and the number and location of collisions they experience in the sheath.

In inductive discharges, the plasma potential is predominantly DC. Normally, this DC potential has only a small AC component superimposed on it due to stray capacitances between the rf induction coil and the plasma. Inductive discharges are normally operated at lower pressure (below 0.1 Torr) and high electron density ($n_e = 10^{11}$ to 10^{12} /cm^3) where the sheaths are narrow. We also expect these sheaths to be collisionless, since total ion-neutral collision cross-sections [40] for argon are less than or equal to 6×10^{-15} cm^2, which leads to an ion mean free path of about 0.5 cm for 10 millitorr discharges, about a factor of 50 larger than the sheath thickness. As a result, in inductive discharges, ions will have a relatively narrow energy distribution (a few eV or less) at the edge of the sheath caused by collisions in the pre sheath, thermal energy and spatial variations in the plasma potential. This distribution will then be uniformly shifted to higher energy, resulting in distributions like those in Fig. 5 as all the ions gain an energy equal to the DC sheath voltage in crossing the sheath.

As mentioned above, the only oscillations in the plasma potential in our inductive discharges will come from stray capacitive coupling between the rf coil and the discharge. These oscillations however, are the most probable cause of the splitting of the energy distributions seen in the mini-detector in Fig. 7. Because of the plasma oscillations, ions entering the sheath at different phases of the RF cycle will arrive at the bottom electrode with different energies. We will only see a splitting of the ion energy distribution for cases with high densities and small sheaths where ions can cross the sheath in less than one rf cycle. For lower densities and larger sheaths, ions will see more than one rf cycle while crossing the sheath and the ion energy distribution will simply broaden, rather than splitting. The data in Figure 7 indicates that the plasma potential is oscillating by about 2.5 Volts, or about 10% of its total value. As the detector is moved off center, the electron density drops, the sheath broadens and the splitting washes out as expected.

To gauge the impact of plasma potential oscillations on the ion energy distribution, we inserted a Faraday shield on the bottom of our window holder, between the rf coil and the discharge (fig. 1) for one experiment. This coil consisted of a copper ring with a number of spokes projecting towards (but not meeting in) the center of the ring and was similar to the Faraday shield described by Mahoney et. al.[18] Using a capacitive pickup probe in the evacuated GEC reference cell, we found that the Faraday shield reduced capacitive coupling between the coil and the discharge region by about a factor of 40. Using the isolated detector, we then re-measured ion energy distributions in argon with the Faraday shield in place. We obtained the same energies and fluxes as without the shield, but the

widths of the distributions were uniformly reduced to 2.1 eV from their value of 2.8 eV without the shield.

It is helpful to compare our data to Langmuir probe measurements by Miller, Hebner, Greenberg, Pochan and Aragon.[34] Graphs presenting electron density and plasma potential from Miller's work are shown in Fig. 10 for 10 millitorr argon discharges with 150 Watts rf input power. These measurements were taken in a GEC reference cell which was nominally identical to the one used in our work. First, we will compare the measurments of plasma potential. The mini-detector measurements were taken with the detector 1.9 cm above the lower electrode and gave a plasma potential of 20.5 eV in the center of the discharge, in excellent agreement with Miller et. al. The isolated detector measurements should reflect the value of the plasma potential one ion mean-free-path above the lower electrode, about 5 mm in this case. The isolated detector value of 18.5 eV is also in excellent agreement with the Langmuir probe data.

Second, we can compare the flux measurements from the two analyzers. For 10 millitorr Ar and 150 Watts input power, the isolated detector sees a total ion flux of 10.9 milliamps/cm^2 and the mini-ion detector sees 12.5 milliamps/cm^2. Since the mini-ion detector is in the densest part of the discharge and the isolated detector is below the bottom electrode, this is excellent agreement. Further, in several different discharges in which the absolute fluxes changed by a factor of five, the ratio of the fluxes seen by the isolated and mini-ion detectors changed by less than 1%.

Third, although the analysis is not as simple, we can compare our total ion flux measurements to Miller's electron density measurements. We note that Miller suggests his Langmuir probe electron density measurements need to be multiplied by 1.25, based on comparison of his results to microwave interferometer results. We know that the product of ion density and velocity will remain constant throughout the plasma sheath[1]. The measurements with the isolated detector tell us the ion density and velocity at the lower electrode. If we can estimate the ion velocity at the edge of the sheath, we can calculate the ion density in the plasma to compare with Miller et. al.[34] From the total ion flux of 10.9 mA/cm^2, the mean ion energy of 18.5 eV and $E = 1/2\ mv^2$, we calculate that there were 7.4×10^{10} ions/cm^3 at the bottom electrode, with an average velocity of 9.2×10^5 cm/sec. We can estimate the ion velocity at the sheath edge either by using the ion thermal (Bohm) velocity: $v = (kT_e / M_{ion})^{1/2}$, or by using values of the drift velocity of argon ions in argon measured by Hornbeck [40,41] as a function of E/p. We estimate E as 10 V/cm near the sheath using Miller's data by taking the gradient of his measured plasma potential near the lower electrode. Using the Bohm velocity, we calculate an ion velocity at the sheath edge of 3×10^5 cm/sec and an ion density of 22×10^{10} /cm^3. Using Hornbeck's data, we calculate an ion velocity at the sheath edge of 2.5×10^5 cm/sec and an ion density of 27×10^{10} /cm^3. Miller's value of the electron density at the lower sheath edge (after being multiplied by 1.25) is 24×10^{10}/cm^3 in excellent agreement with our estimates of 22 to 27×10^{10} ions/cm^3.

Figures 11 and 12 show the radial variation of ion energy and ion flux in 5 and 10 millitorr argon discharges as measured by the mini-ion detector. Miller's Langmuir probe values

for the plasma potential in a 10 millitorr Ar discharge are shown in figure 12 for comparison. The shape of the ion flux curve in figure 11, which is peaked on the centerline and falls to one-half its centerline value 4 cm from the axis, is also in agreement with Miller's data.

The widths of the ion energy distributions we measure with the ion detectors have a number of contributing components, including: the energy resolution of the detectors, the thermal energy distribution of the ions in the bulk plasma, oscillations in the plasma potential, and spatial variation in the plasma potential in the pre sheath. With no Faraday shield in place, the isolated detector consistently saw ion energy distributions with a 2.8-eV FWHM, independent of pressure or rf power. The Faraday shield eliminated the plasma potential oscillations and reduced the width of the distribution to 2.1 eV. From the work of Miller et. al.[34] (Fig. 10) the plasma potential varies by about 2 volts in the last 5 mm (one ion mean free path) above the grounded electrode, which should result in about a 2-eV spread in the ion distribution seen at the electrode. We know from separate experiments with chlorine discharges that the resolution of the isolated detector is less than 1.4 eV. The thermal energy distribution of the ions in the bulk plasma as measured by Hebner[42] is less than 0.1 eV and is negligable compared to the other sources of energy spread in the ion energy distribution. We conclude from this, that with the Faraday shield in place to suppress the plasma potential oscillations, most of the width of the ion energy distribution functions we measured with the isolated detector was caused by spatial variations in the plasma potential.

The shape of the ion energy distributions we see is in good agreement with the shapes predicted by Kortshagen and Zethoff[21] and by Riemann[42] for a purely inductive discharge with a collisional pre-sheath. The mean energies of our distributions, however, depend more strongly on pressure than Kortshagen's work predicts. Our mean energies agree with his predictions at 15 mTorr, but are 12 eV higher than his predictions at 2.5 mTorr.

B. Ion Angular Distributions:

In measuring ion angular distributions, it is important to determine that the ion trajectories are not perturbed by fringing electric fields around the pinhole. This problem is particularly severe in the high density discharges studied here since the sheaths are very narrow and hence sheath E-fields are very high. To investigate this phenomenon empirically, we took the data in Fig. 13, which shows normalized plots of ion angular distributions versus pinhole size. While Fig. 13 clearly shows a "smearing" of the ion angular distribution for pinholes of 30 and 75 microns, the distribution is approximately constant for pinholes of 10 micron diameter and smaller. In addition, we note that for the smaller pinholes, the area-normalized signal, obtained by dividing the signal from each annular electrode by the electrode area, becomes monotonically decreasing with angle from the pinhole normal (see Fig. 15). This is the expected appearance of any real angular distribution from these discharges. The rest of the angular data we present here is with the smallest pinhole, a 2-micron-diameter pinhole in a 1.5-micron-thick gold foil. We have corrected for the finite thickness of this pinhole foil as discussed in Section II B. Figure

14 shows a series of ion angular distributions for a variety of argon pressures and 200 Watts of rf power entering the rf matching network. It is clear from this picture that both the width of the angular distribution and the total flux increase with pressure.

If we assume that the distribution function of the ions at the pinhole can be approximated by a drifting Maxwellian distribution[44], we can derive estimates of the ratio of the transverse to longitudinal temperatures of the ions from our data. The measured ion current per detector electrode area is fit to a simple functional form:

$$J = A[\cos^4(d)]\exp[-B\sin^4(d)]$$

where d is the mean angle and A and B are to be determined by the fit. B is defined as E_d/kT_t where E_d and T_t are the directed energy ($E_{directed} = 1/2\ mV^2$) and the transverse temperature (kT_t). Figure 15 shows fits of three of the curves in figure 14 to drifting Maxwellians. In general, the fits are best at low pressures and powers. Figure 16 shows the trends in our angular data, displaying data for $E_{directed}$, $kT_{transverse}$ and the ratio of $E_{directed} / kT_{transverse}$. The transverse temperature is a function of pressure, increasing from 0.29 eV to 0.5 eV when the pressure increases from 2.9 mTorr to 50 mTorr at 200 Watts rf input power. The transverse temperature is also a weak function of power, increasing from 0.20 to 0.33 eV at 2.9 mTorr when the rf power increases from 100 to 300 watts.

As a second test of the effect of pinhole size on our results, Fig. 17 shows our measured transverse energies as a function of pinhole size. The results for the 5 and 2 micron pinholes are essentially identical (i. e. they are within 17% of each other) over the full range of pressures we tested. The 10 micron pinhole data data at high pressures, however, are 50 % higher than the results with the smaller pinholes. From these results, we conclude that while the 10 micron results were affected by the fringing fields around the pinhole, the 5 and 2 micron data were not significantly affected.

It is useful to compare our angular results to the transverse temperature measurements of Hebner[42]. Hebner used laser-induced fluorescence to measure ion transverse temperatures in the bulk plasma of an argon discharge in an identical GEC reference cell. For 200 Watts rf input power, Hebner measured ion temperatures varying from 0.07 to 0.09 eV, about a factor of five lower than the temperatures we measure. We conclude from this that the ion angular distribution is considerably broadened, probably by collisions, as the ions pass through the pre-sheath region.

Finally, we looked at the ion energy distributions as a function of angle. Figure 18 shows ion energy spectra as detected by six different collector rings on our detector for a 10-mTorr, 200-Watt rf discharge in argon. To first order, the ion energy distributions appear to be independent of the angle at which the ions strike the lower electrode. Figure 18 does show a slight shift to higher ion energies (about 0.5 eV)for the ions passing through the pinhole 12 to 20 degrees off axis, but this shift is smaller than the 2.8 eV full-width-at-half-maximum of the ion distributions.

VI. Conclusions:

Our work allows us to draw several conclusions about the spectra we see in these inductively coupled argon plasmas. First, each ion energy distribution consists of a single feature which is well separated from zero energy. This is very different from the spectra seen in capacitively coupled discharges and reflects the quiescent nature of the plasma sheath and plasma potential in inductively coupled discharges. Second, we find that the ion energies are independent of rf power, but vary inversely with pressure. Third, the discharge is fairly non-uniform: The ion energies vary by 40% from the center to the edge of our 15.2 cm diameter electrode and the ion fluxes vary by more than a factor of five. Fourth, we find that our ion energy and flux measurements are in good agreement with electron energy and flux measurements measured with a Langmuir probe. Fifth, the splitting in the ion energy distributions seen by the mini-ion detector indicates that the plasma potential in our discharge has an oscillating component (about 2.5 Volts peak-to-peak) superimposed on a DC potential of about 20 Volts. The oscillating portion of the plasma potential is probably caused by stray capacitive coupling between the induction coil and our discharge. Finally, the full-width-at-half-maxima of the ion energy distributions do not change with pressure or rf power, remaining constant at 2.8 eV. Eliminating the stray capacitive coupling between the rf coil and the plasma, however, does reduce the FWHM to 2.1 eV.

We can also draw several conclusions about ion angular distributions. First, the angular distributions appear to be controlled by two independent parameters. The width of the distributions increases as either power or pressure increase. Second, the distributions are fairly narrow, with half-widths that vary from 5 degrees to 12.5 degrees for our experiments. If we fit the distributions to drifting Maxwellian distributions, this corresponds to a range of $E_{directed} / kT_{transverse}$ varying from 120 to 20. Finally, our measurements of ion transverse temperature are a factor of 4 to 5 higher than transverse temperatures measured in the bulk plasma, indicating that most of the ion's transverse energy seen at the electrode is acquired in its passage through the pre-sheath region.

V. Acknowledgements:

We wish to thank Paul Miller and Greg Hebner (Sandia National Laboratories) and Prof. Mark Kushner (Univeristy of Illinois, Urbana) for a number of helpful discussions. We also wish to acknowlege the support of Sandia's Thin film & Brazing, Project Machining/Rapid Turnaround, and Electronic Processing teams who fabricated many of the parts for the isolated ion analyzer and our modified GEC reference cell. We are grateful for the support for this work provided by the U. S. Department of Energy under contract DE-ACO4-94AL85000 and by SEMATECH.

References:

1. Dry Etching for VLSI, A. J. vanRoosmalen, J. A. G. Baggerman, and S. J. H. Brader. Plenum Press, New York, 1991.

2. Principles of Plasma Discharges and Materials Processing, Michael A. Lieberman, Allan J. Lichtenberg, John Wiley & Sons, New York, 1994

3. Silicon Processing for the VLSI Era: Volume I - Process Technology, S. Wolf and R. N. Tauber, Lattice Press, Sunset Beach, California, 1987

4. J. E. Johannes, T. J. Bartel, R. S. Wise, D. J. Economou, paper PS-MoM7: Comparison of Low Pressure Cl_2 Plasma Simulations With Experimental Data in an Inductively Coupled Source, 42nd National Symposium of the American Vacuum Society, Minneapolis MN, October 16, 1995

5. R. J. Hoekstra and M. J. Kushner; Predictions of Ion Energy Distributions and Radical Fluxes in Radio Frequency Biased Inductively Coupled Plasma Etching Reactors, Journal of Applied Physics, in press 1996.

6. C. Lee and M. A. Lieberman, J. Vac. Sci. Technol. A (**13**)2, March/April 1995, p 368

7. E. F. Jaeger, L. A. Berry, J. S. Tolliver and D. B. Batchelor, Physics of Plasmas **2** (6) June 1995, p. 2597

8. E. Meeks and J. W. Shon, J. Vac. Sci. Tech. A **13**, (1995), p. 2884

9. B. Lipschultz, I. Hutchenson, B. LaBombard, and A. Wan, J. Vac. Sci. Technol. **A4** (3) May/ June 1986, p. 1810

10. Principles of Plasma Diagnostics, I. H. Hutchenson, Cambridge University Press, New York, 1992, p. 80

11. J. A. Simpson, Review of Sci. Instruments, **32** (12) December 1961, p. 1283

12. J. Liu, G. L. Huppert, and H. H. Sawin, J. Appl. Phys **68** (8), 15 Oct. 1990, p. 3916

13. Scaling Relationships for Power Deposition and Ion Bombardment in Radio-Frequency Plasmas, Joanne Liu, MIT PhD thesis, 1993, Available from MIT Document Services, Rm 14-0551, 77 Mass. Ave Cambridge, Mass. 02139-4307, (617)-253-5668

14. B. E. Thompson, K. D. Allen, A. D. Richards, and H. H. Sawin, J. Appl. Phys. **59** (6), 15 March 1986, p. 1890

15. U. Flender and K. Wiesemann, J. Phys. D: Appl. Phys **27** (1994) p. 509

16. A. Wild and P. Koidl, J. Appl Phys. **69** (5) 1 March 1991, p. 2909

17. S. G. Ingram and N. St. J Braithwaite, J. Phys D: Appl Phys. **21** (1988) p. 1496

18. L. J. Mahoney, A. E. Wendt, E. Barrios, C. J. Richards, J. Appl. Phys, 76(4) , 15 August 1994, P. 2041

19. S. M. L. Prokopenko, J. G. Laframboisie and J. M. Goodings, J. Phys D: Appl Phys **7** (1974) p. 355

20. J. Hopwood, Appl. Phys. Lett **62** (9), 1 March 1993, p. 940

21. U. Kortshagen and M. Zethoff, Plasma Sources Sci. Technology, **4** (1995), p. 541

22. Radial Ion Transport in a limited Axisymmetric ECR Plasma, Gerald Gibson, Jr., MIT PhD. thesis, 1994,

23. Ion Energy Distribution Functions Perpendicular and Parrallel to the Magnetic Field in ECR Plasmas, Minh Sy Le, MIT B.S. Thesis, 1995

24. F. Matthews, J. Phys. D: Appl. Phys. **17** (1984), p. 2243

25. A. W. Molvik, Rev. Sci. Instrumen. **52** (5) May 1981, P. 704

26. Ion Energy Measurements in an Inductive RF Plasma with RF Bias, John Trow, Applied Materials, 47th Annual Gaseous Electronics Conference, Gaithersburg MD, October 1994

27. W. D. Davis and T. A. Vanderslice, Phys. Rev, **131** (1) July 1, 1963, p. 219

28. A. Manenschijn, E. van der Drift, G. C. A. M. Janssen and S. Radelaar, J. Appl. Phys. **69** (12), June 15, 1992, p. 7996

29. W. M. Greene, M. A. Hartney, W. G. Oldham and D. W. Hess, J. Appl. Phys. **63** (5) March 1, 1988, p. 1367

30. J. K. Olthoff, R. J. VanBrunt, and S. B. Radovanov, J. Appl, Phys, 72 (1992) p. 4566

31. J . K. Olthoff, R. J. VanBrunt, and S. B. Radovanov "Studies of Ion Kinetic Energy Distributions in the Gaseous Electronics Conference RF Reference Cell", Journal of Research, National Inst. of Standards & Technology, **100** (4) July-August 1995

32. P. J. Hargis, Jr. , K. E. Greenberg, P. A. Miller, J. B. Gerardo, J. R. Torczynski, M. E. Riley, G. A. Hebner, J. R. Roberts, J. K. Olthoff, J. R. Whetstone, R. J. Van Brunt, M. A. Sobolewski, H. M. Anderson, M. P. Splichal, J. L. Mock, P. Bletzinger, A. Garscadden, R. A. Gottscho, G. Selwyn, M. Dalvie, J. E. Heidenreich, J. W. Butterbaugh, M. L. Brake, M. L. Passow, J. Pender, A. Lujan, M. E. Elta, D. B. Graves, H. H. Sawin, M. J. Kushner, J. T. Verdeyen, R. Horwath and T. R. Turner, Rev. Sci. Instruments, **65**, (1994) p. 140. P. J. Hargis, Jr. et. al. Rev. Sci. Instruments, **65**, (1994) p. 140

33. J. K. Olthoff and K. E. Greenberg, Journal of Reserach, National Institute of Standards and Technology **100** (4) July-August, 1995, p. 327

34. P. A. Miller, G. A. Hebner, K. E. Greenberg, P. D. Pochan,and B. P . Aragon, Journal of Research, National Institute of Standards and Technology **100** (4), July-August 1995, p. 427

35. The wire screen grids for the isolated detector were obtained from the Unique Wire Weaving Co, Inc, 762 Ramsey Ave. Hillside, HJ 07205, (908)-688-4600

36. P. A. Taylor, J. Vac. Sci. Technology **A6**, (4), July - August, 1988, p. 2583

37. VESPEL™ is a trademark of the DuPont Corporation.

38. Pinholes were obtrained from National Apertures, Inc. 26 Keewaydin Dr. Suite B, Salem NH, (603) 893-7857

39. Screen grids for the mini-ion detector were of electro-formed nickel and were obtained from Buckbee-Mears, Inc. 254 E. 6th St, St. Paul MN, 55101, (612) 228-6400

40. Collision Phenomena in Ionized Gases, Earl W. McDaniel, John Wiley & Sons, New York, 1964, pps. 165 & 464

41. J. A. Hornbeck, Phys Rev. **84**, p. 615 (1951)

42. G. A. Hebner, Journal of Applied Physics, in press

43. K. U. Riemann, Phys. Fluids, 24(12) December 1981, p. 2163

44. F. F. Chen, Introduction to Plasma Physics and Controlled Fusion, second edition, Plenum Press, New York, 1983, P. 231

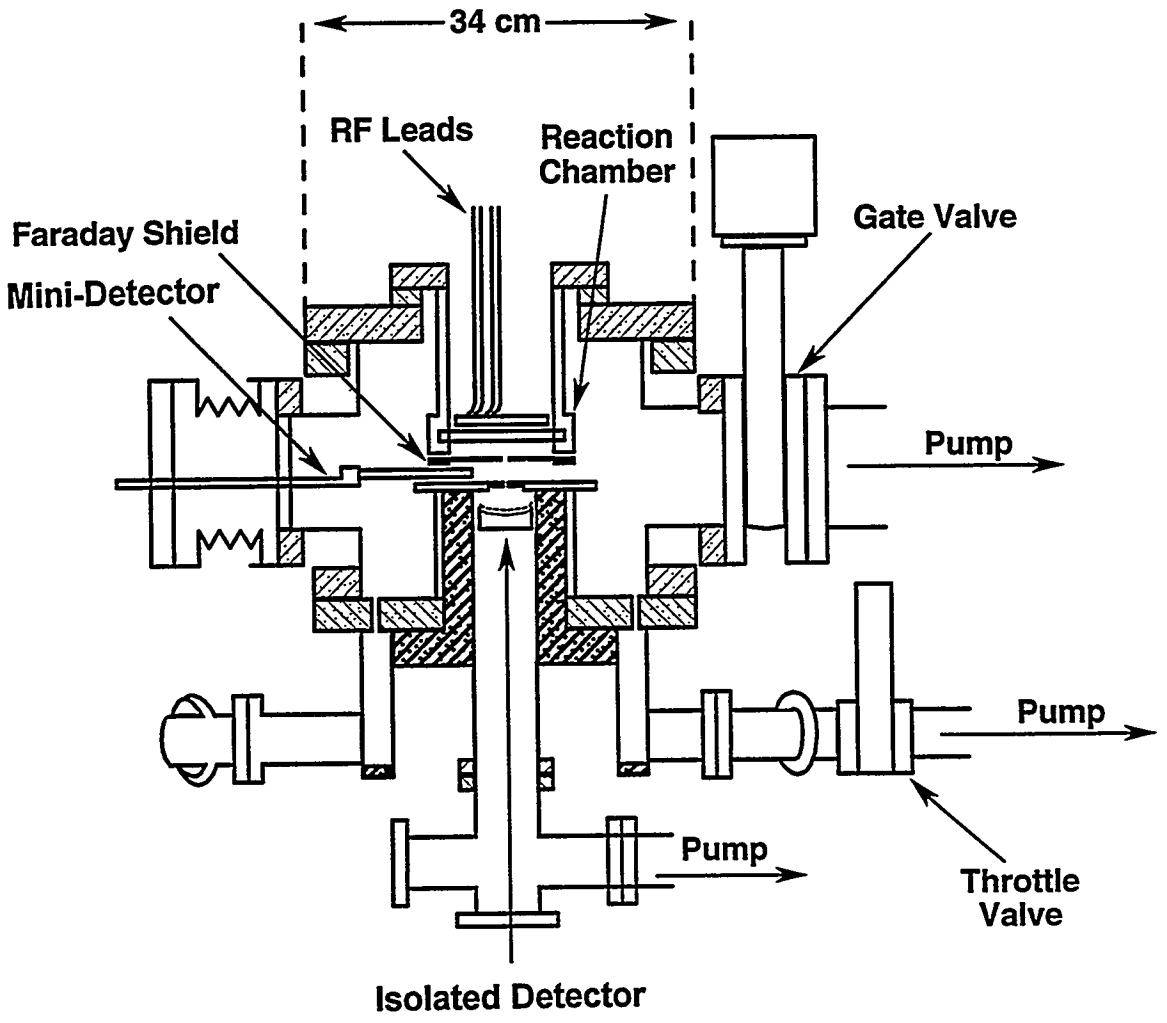

Figure 1: Schematic of the GEC reference cell with inductive RF drive coil. Locations of the two ion detectors are indicated. Location of the faraday shield, which was only used for one experiment, is also indicated.

(Intentionally left blank)

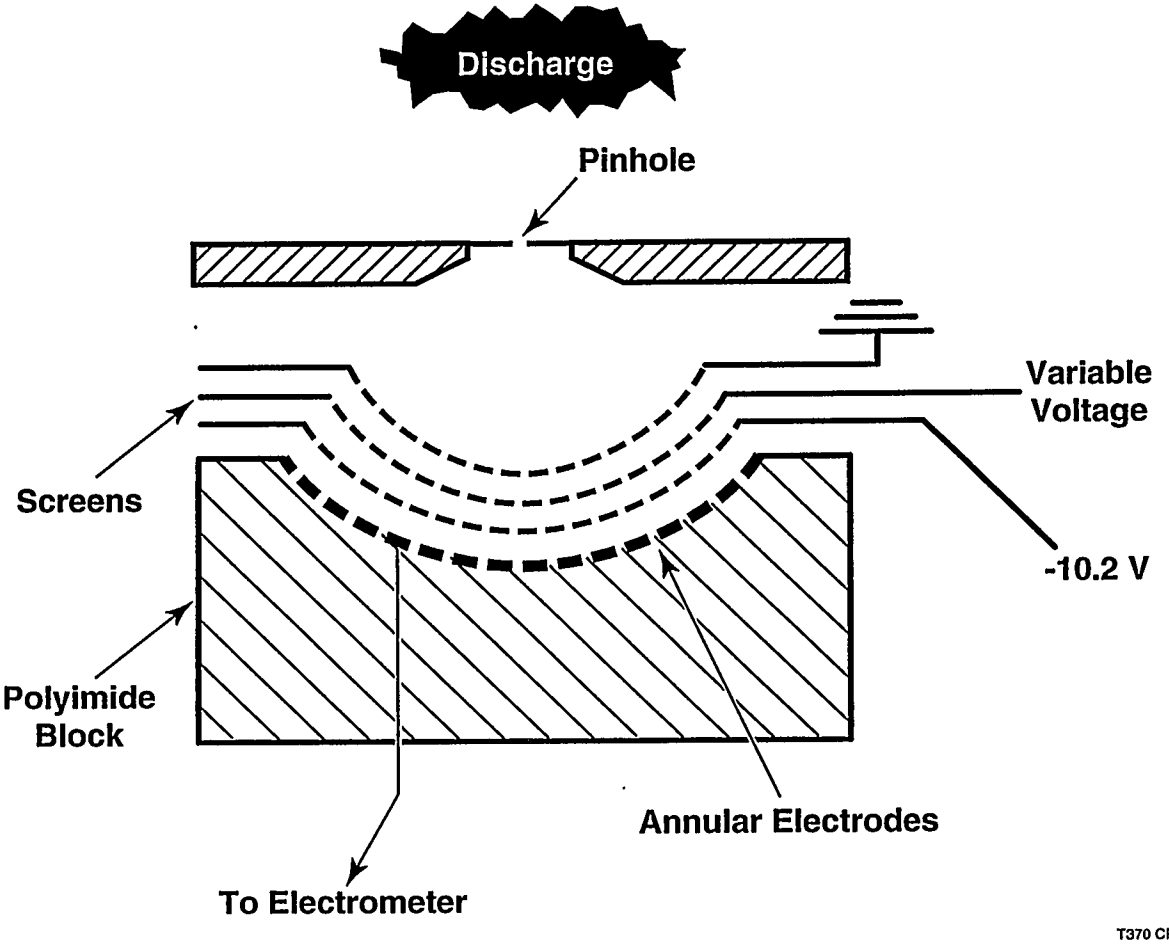

Figure 2. Isolated ion energy and angle analyzer. The three screens and the collection electrodes are sections of concentric hemispheres which are centered on the pinhole. The distance from the pinhole to the annular collection electrodes was 2.29 cm.

(Intentionally left blank)

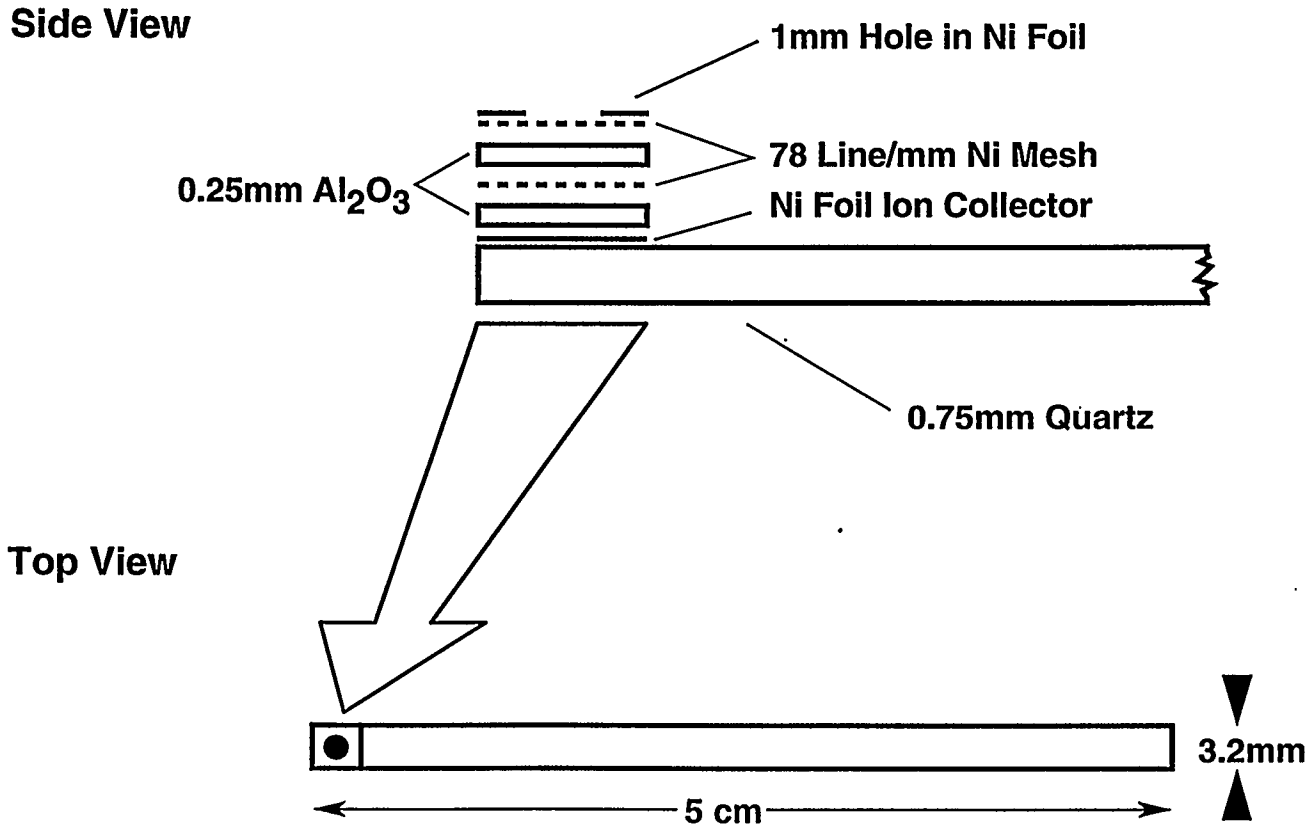

Figure 3. Schematic of miniaturized ion detector. The small size of this detector gives it high spatial resolution and allows it to be mounted on a stalk and moved about in the discharge.

(Intentionally left blank)

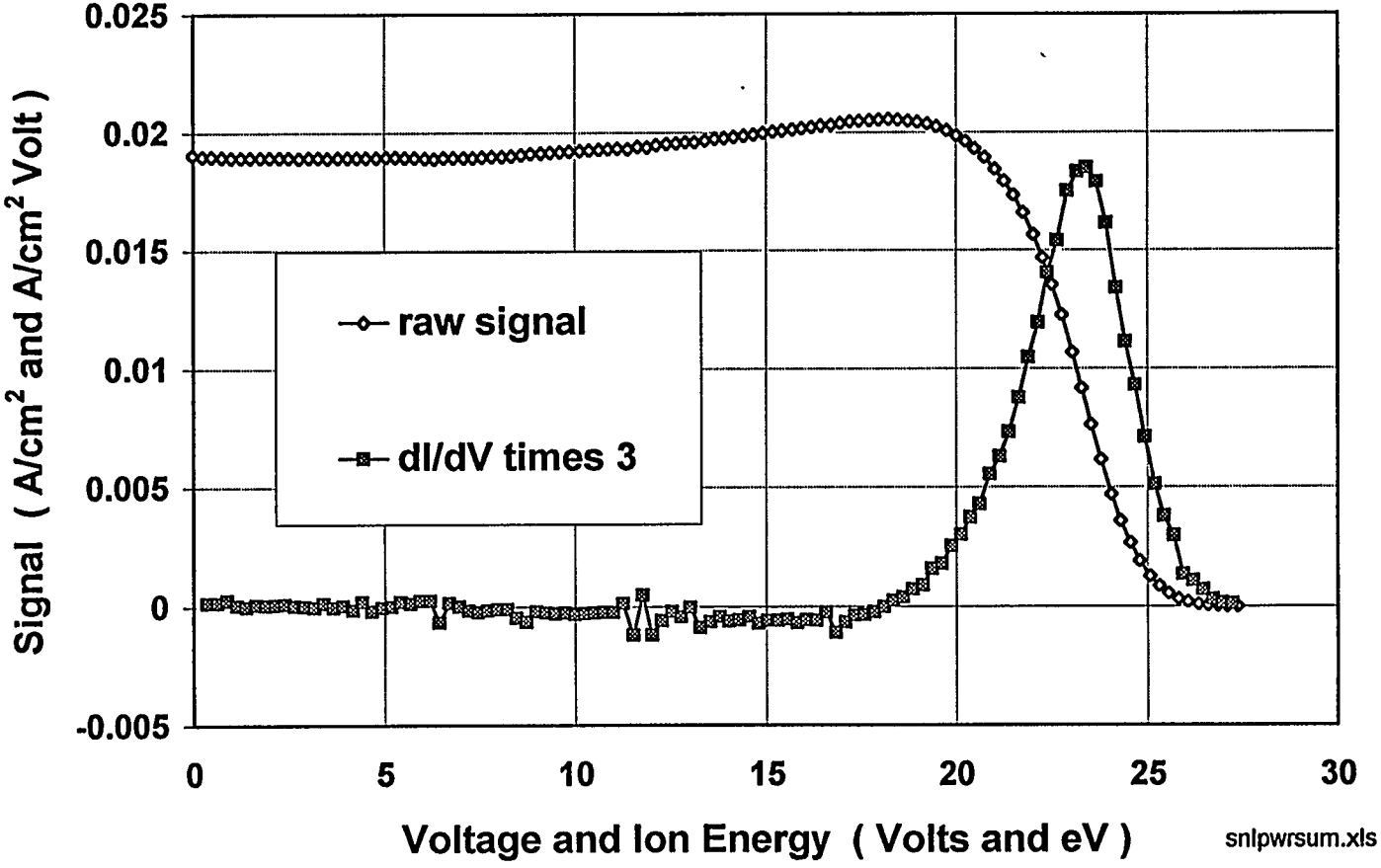

Figure 4. Raw data and ion energy distribution in a 5 millitorr, 300 W, Ar discharge. The ion energy distribution is obtained by differentiating the raw data with respect to voltage.

(Intentionally left blank)

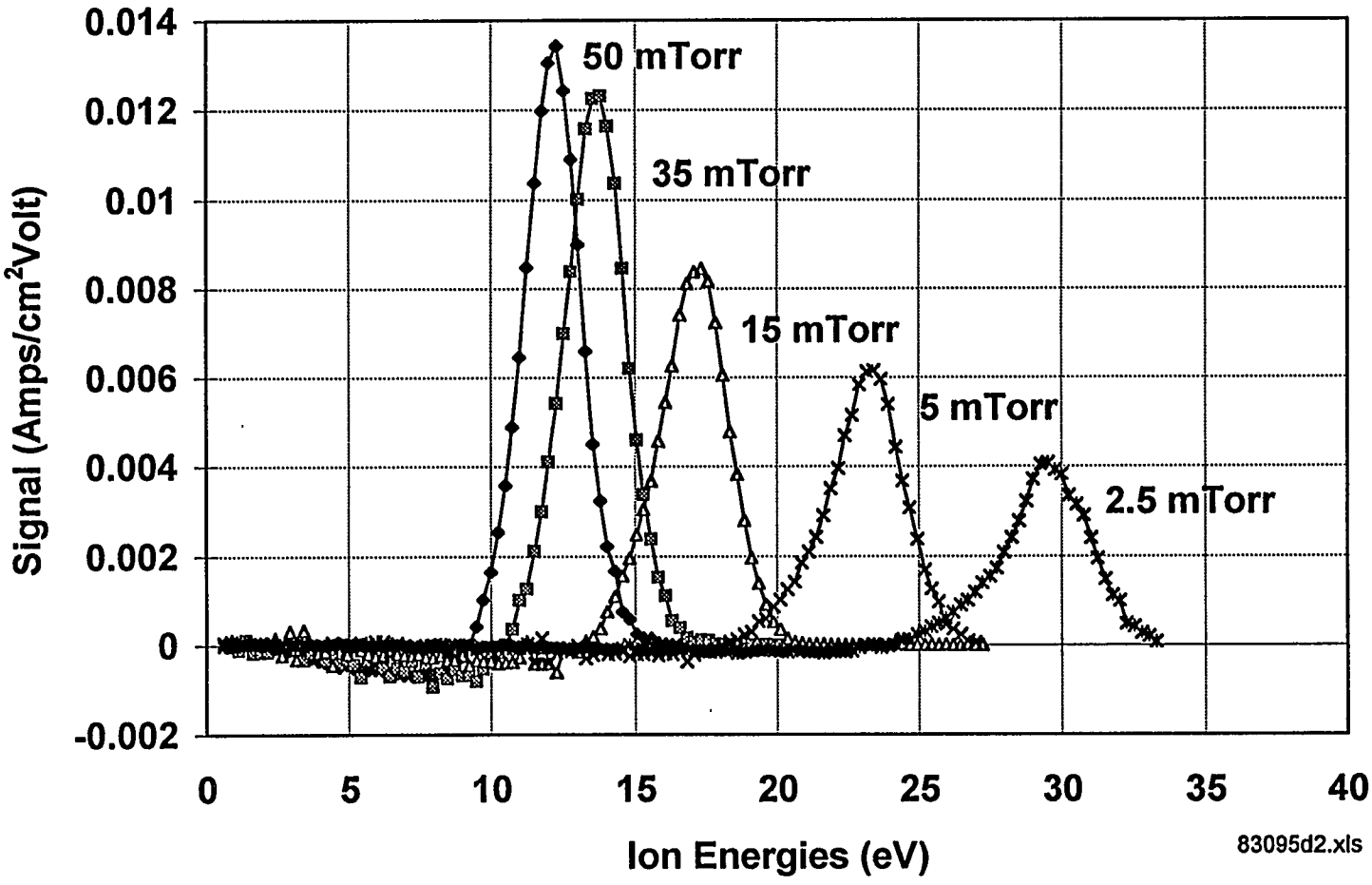

Figure 5. Ion energy distributions in 300 W discharges in Ar as measured with the isolated ion detector and summed over all angles. The mean ion energy decreases with increasing pressure, but the FWHM of the distributions remains constant.

(Intentionally left blank)

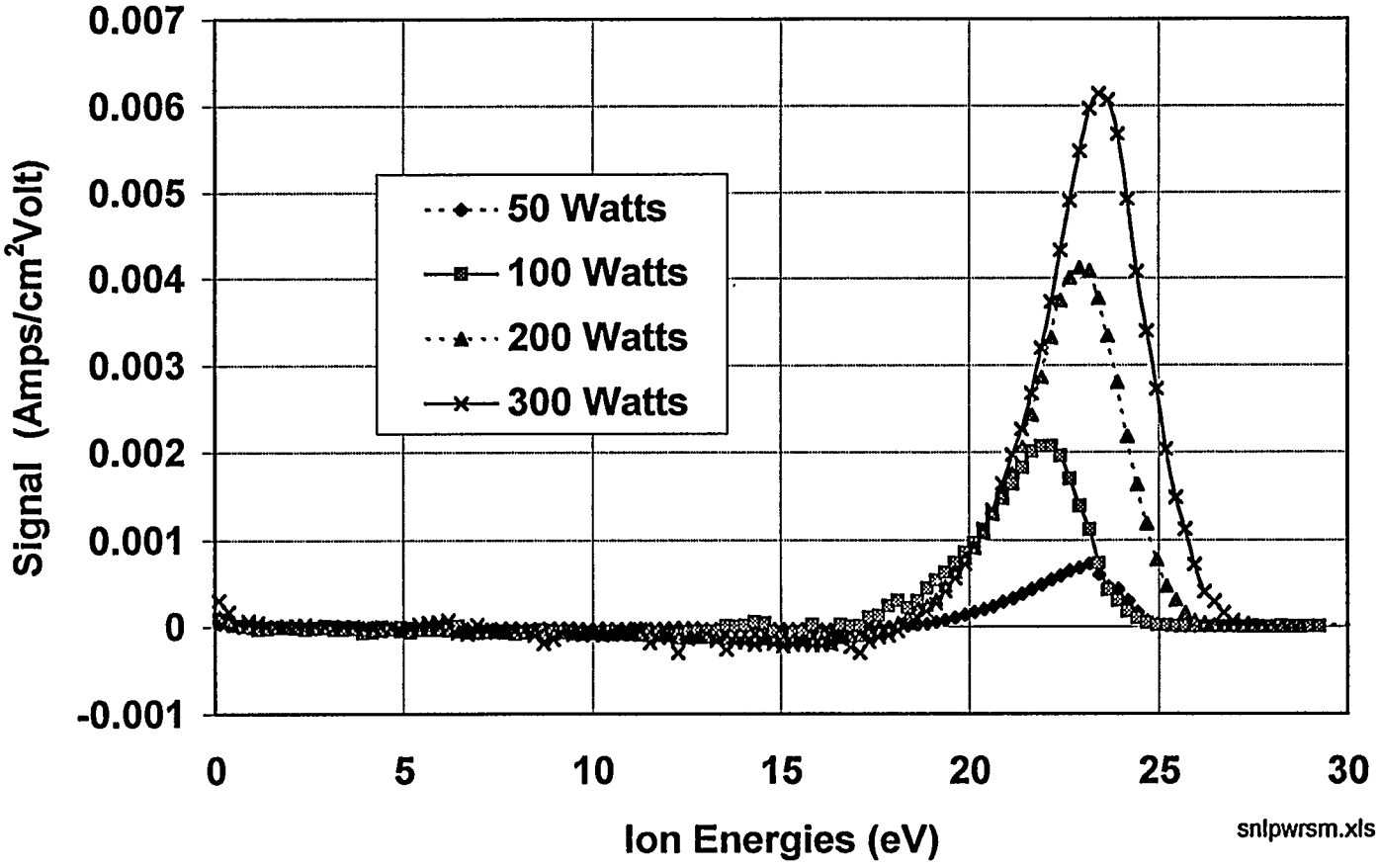

Figure 6. Ion energy distributions in 5 millitorr Ar discharges as measured with the isolated detector and summed over all angles. The mean ion energy and the FWHM of the distribution are independent of RF power.

(Intentionally left blank)

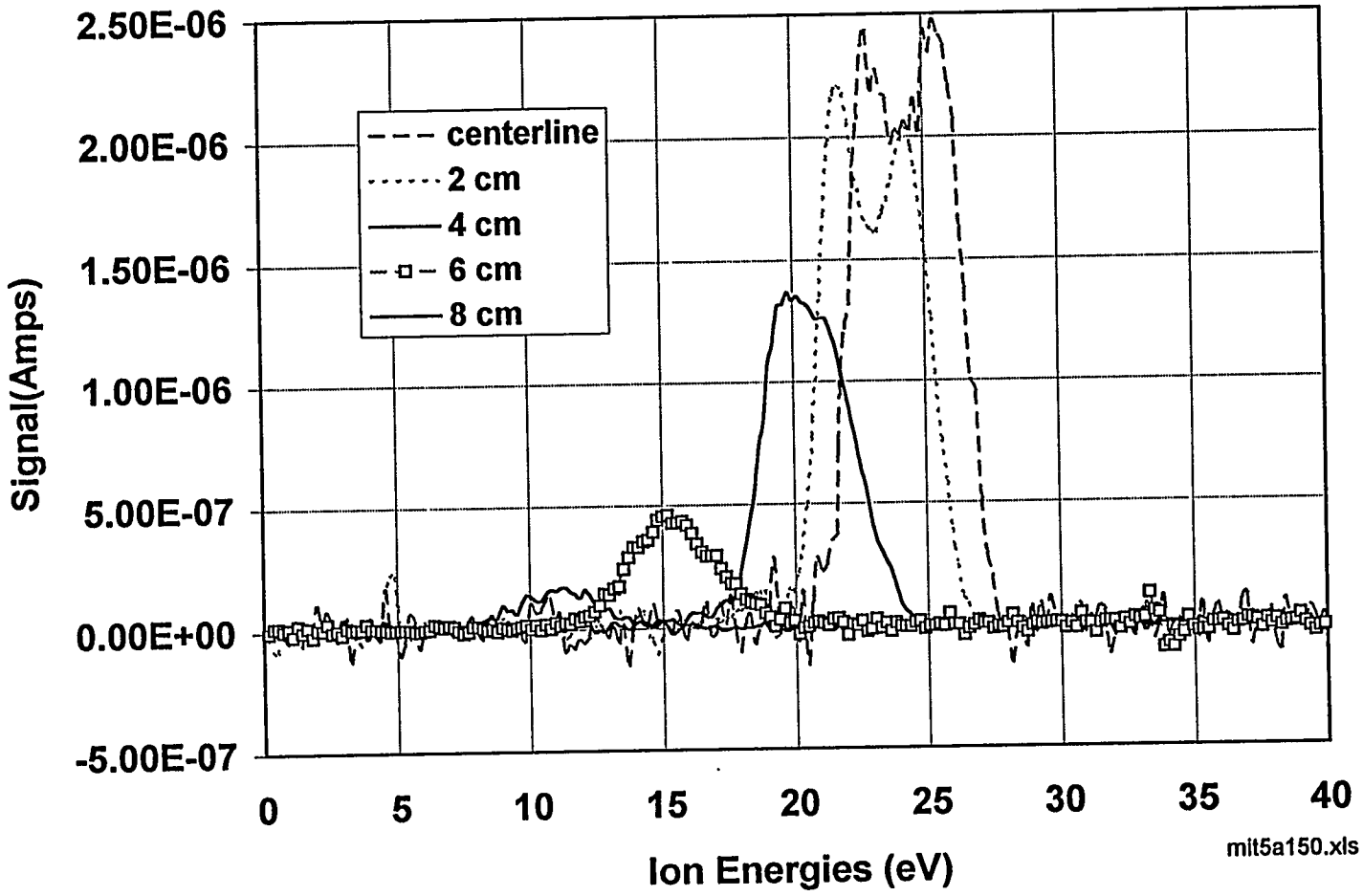

Figure 7. Ion energy distributions versus radius in a 5 millitorr discharge in Ar as measured by the mini-detector. The rf power to the matching network was 150 Watts. As the detector moves off the axis of the discharge, both the ion flux and the mean ion energy decrease and the splitting seen in the distribution on the centerline washes out.

(Intentionally left blank)

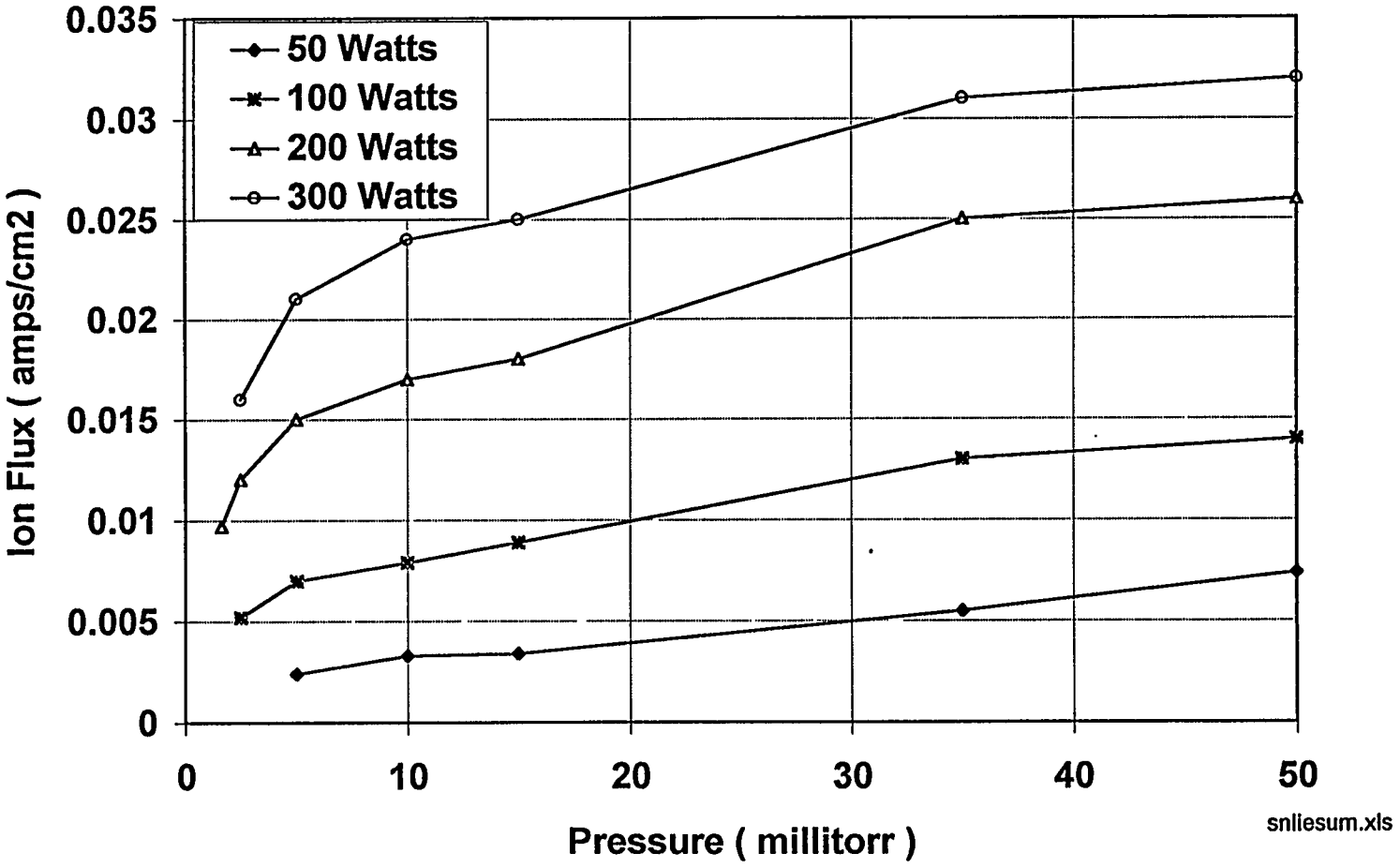

Figure 8. Total ion fluxes in Ar discharges as measured by the isolated detector. Fluxes increase strongly with increases in rf power (powers shown are power to rf matchbox) and weakly with increases in pressure.

(Intentionally left blank)

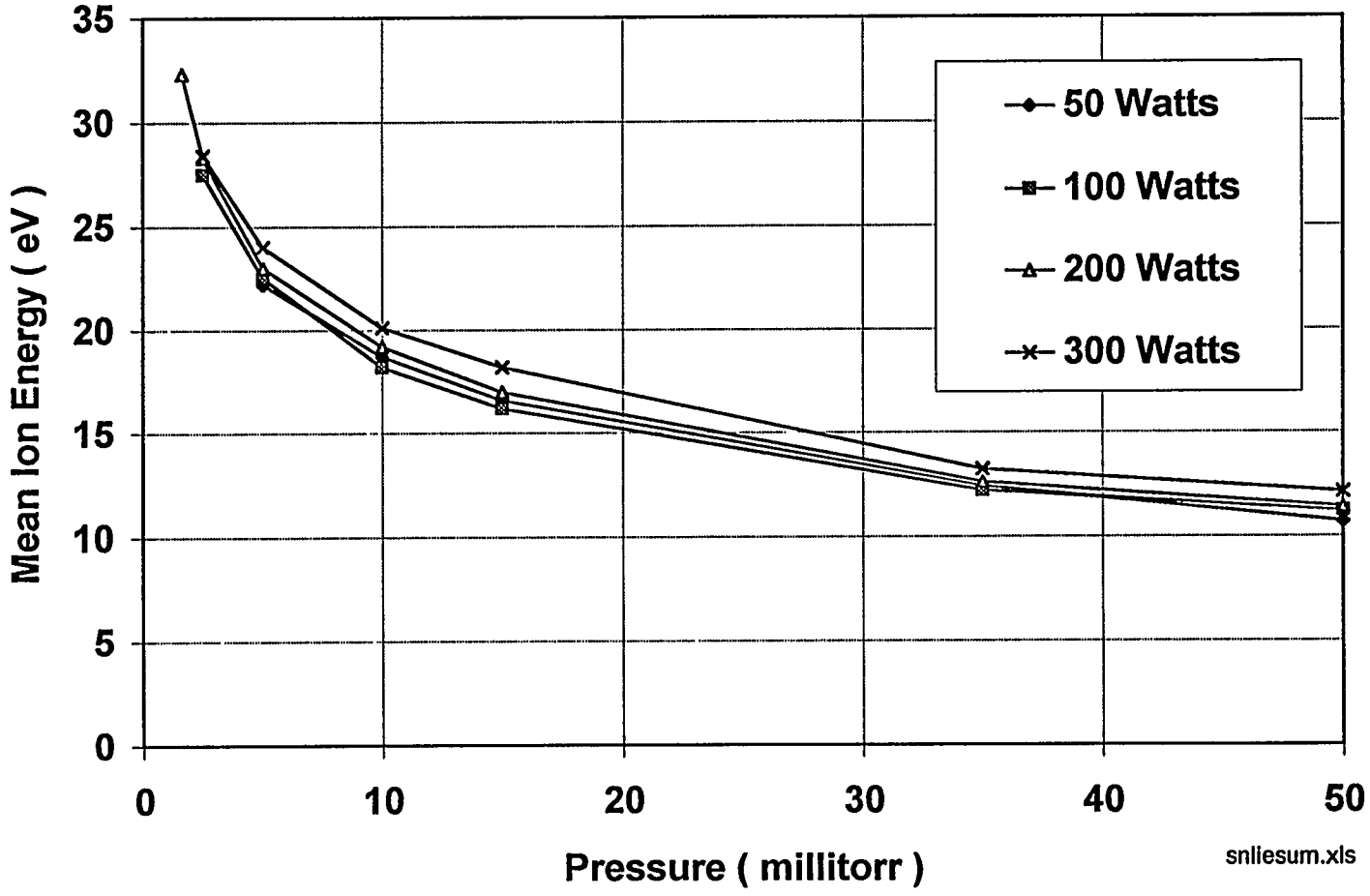

Figure 9. Mean ion energies on the centerline of discharges in Ar as measured with the isolated detector. Note that ion energy is essentially independent of RF driving power. Powers shown are power to the RF matching network.

(Intentionally left blank)

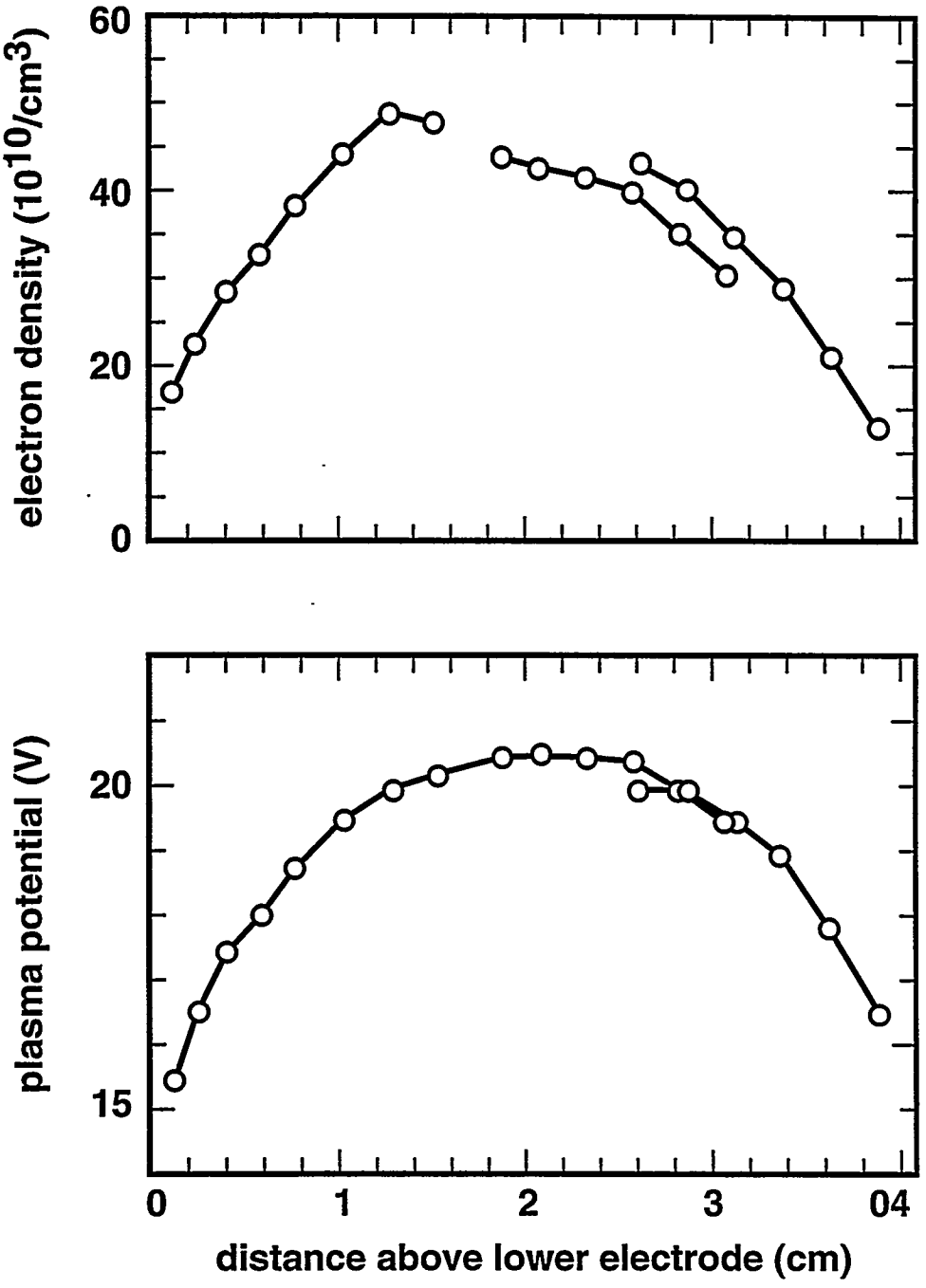

Figure 10. Langmuir probe measurements of electron density and plasma potential taken by Miller et. al. [34] Miller's measurements were taken in a GEC reference cell which was nominally identical to the one used in our experiments.

(Intentionally left blank)

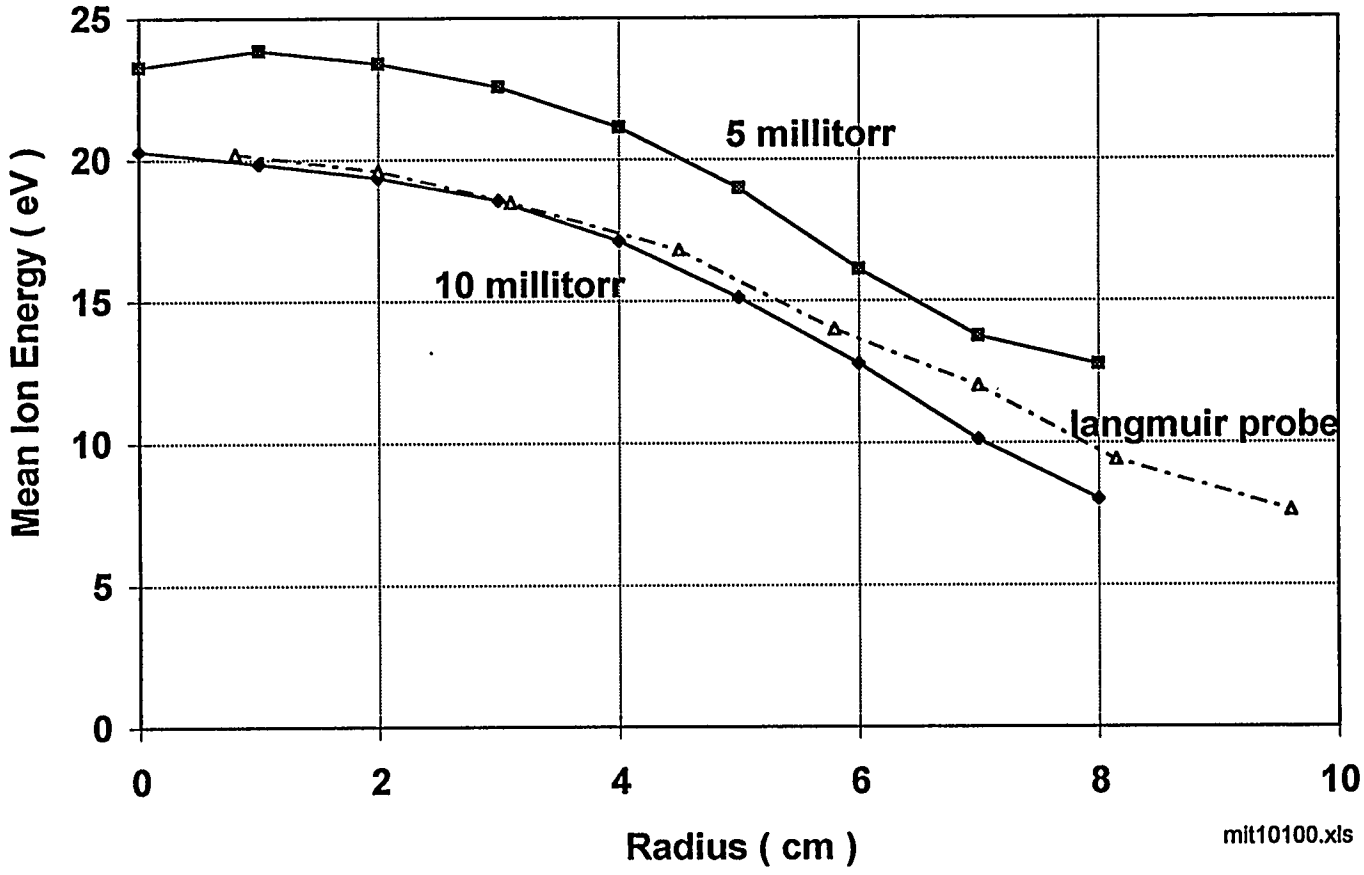

Figure 11. Mean ion energies in argon discharges as a function of radius as measured by the mini-detector. The rf power to the matching network was 100 watts for this data. Langmuir probe data for 10 millitorr, 100-W Ar discharges from Miller's work[29] are shown for comparison.

(Intentionally left blank)

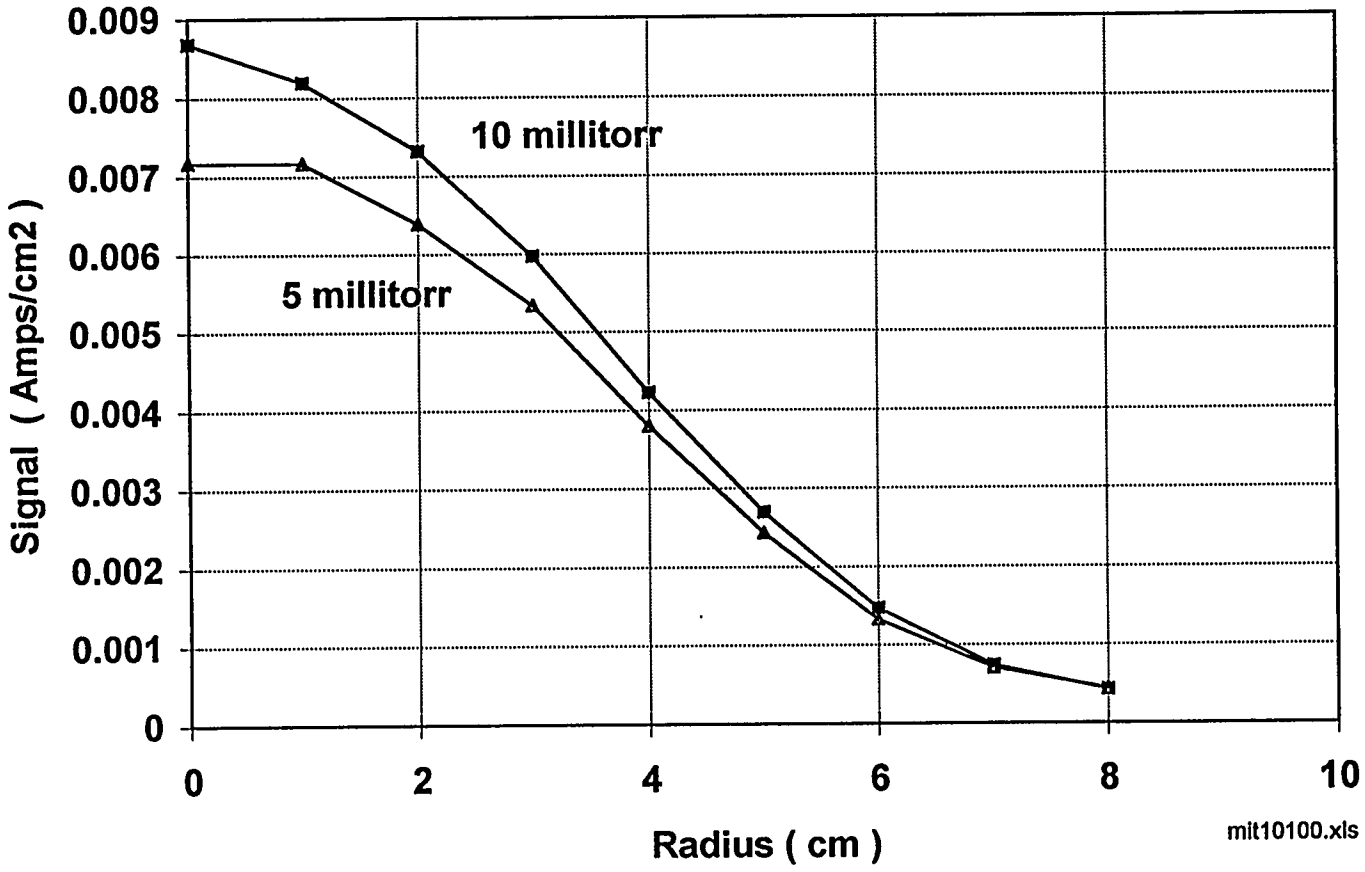

Figure 12. Ion fluxes versus radius for Ar discharges as measured by the mini-detector. The rf power to the matching network was 100 Watts. Note the factor of eight variation in ion flux as the detector moves from the centerline to the edge of the electrode at r = 7.5 cm.

(Intentionally left blank)

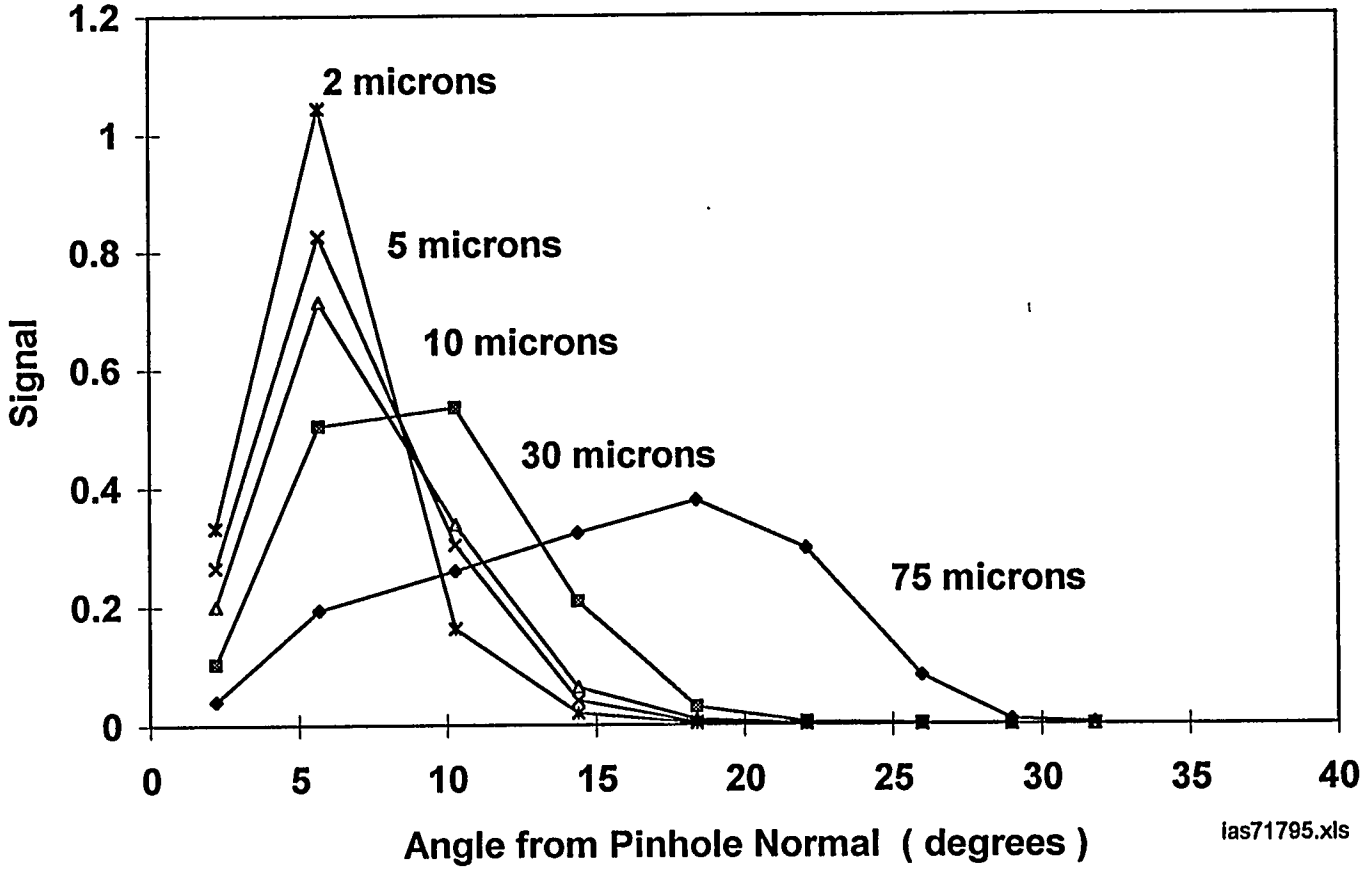

Figure 13. Measured ion angular distributions in 10 millitorr Ar discharges as a function of the size of the pinhole separating the detector from the plasma. The data for 30 and 75 micron pinholes clearly show smearing of the distriubtions due to fringing fields around the large pinholes. RF power to the matching network was 150 Watts for this data.

(Intentionally left blank)

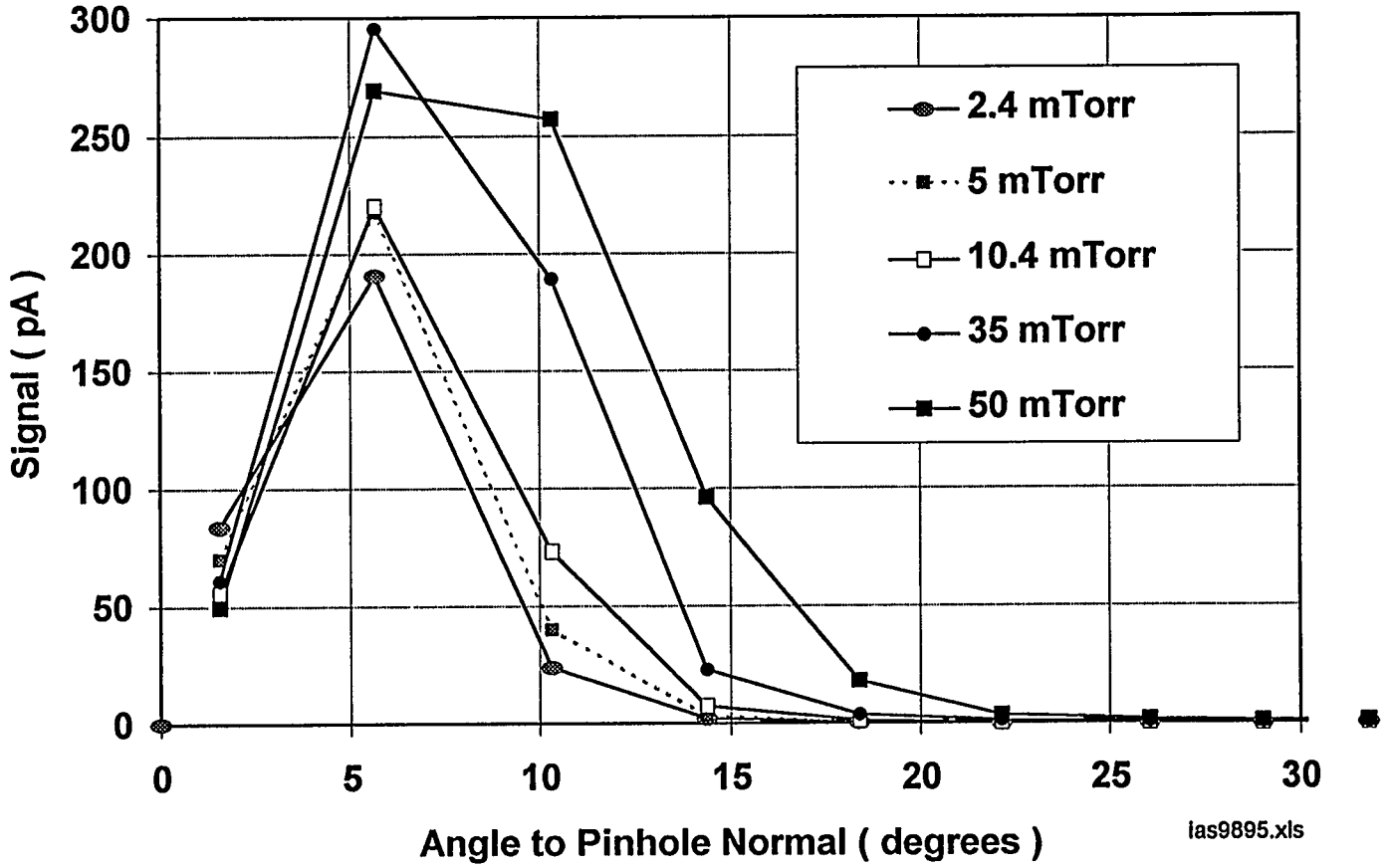

Figure 14. Ion angular distributions for discharges in Ar as a function of discharge pressure. Note that the flux increases and the distribution broadens as the pressure increases. A 2-micron diameter pinhole was used for these measurements and the rf power to the matching network was 200 Watts.

(Intentionally left blank)

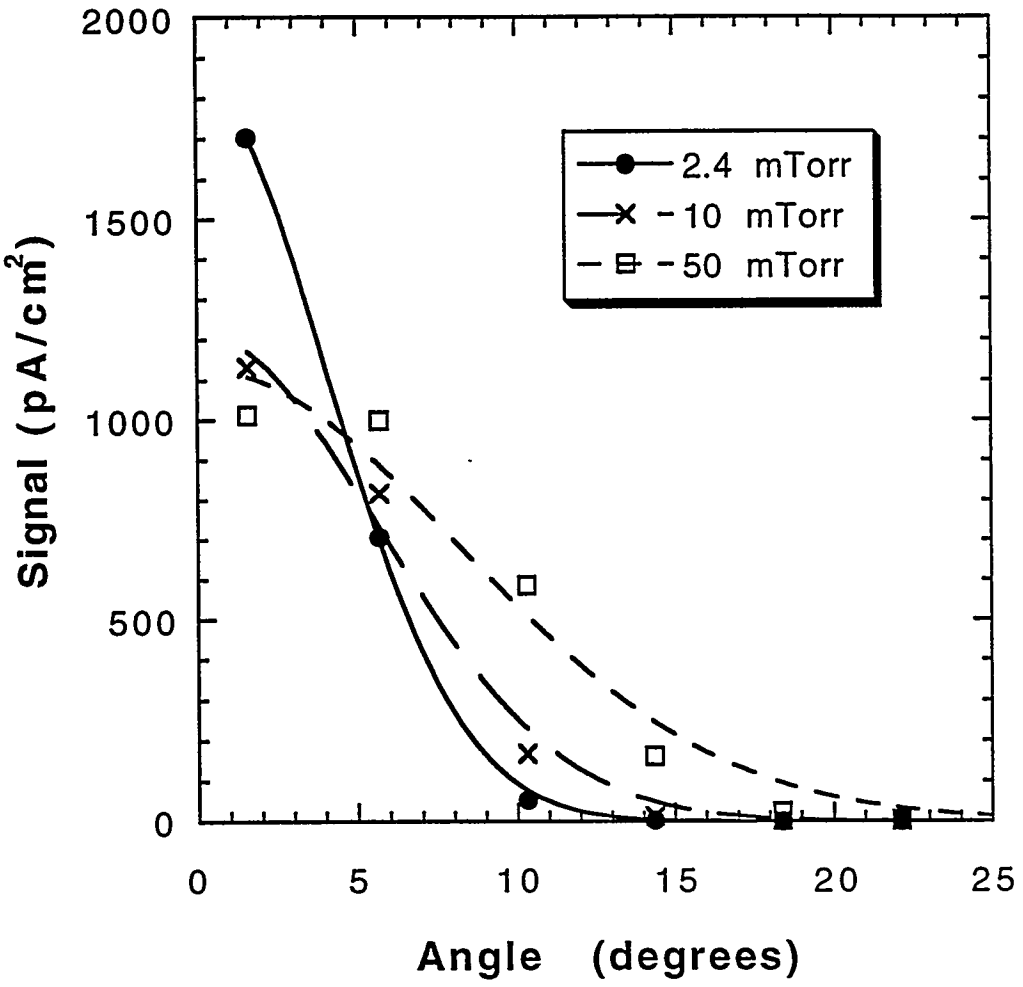

Figure 15. Drifting Maxwellian distribution fits to three of the ion angular distribution curves shown in figure 13. These fits allow us to assign a "transverse temperature" to the ion distribution as explained in the text. Note that the signals shown here are current per cm^2 of collector area on the various ring electrodes of the isolated ion analyzer. In general, the fits are best at low powers and pressures.

(Intentionally left blank)

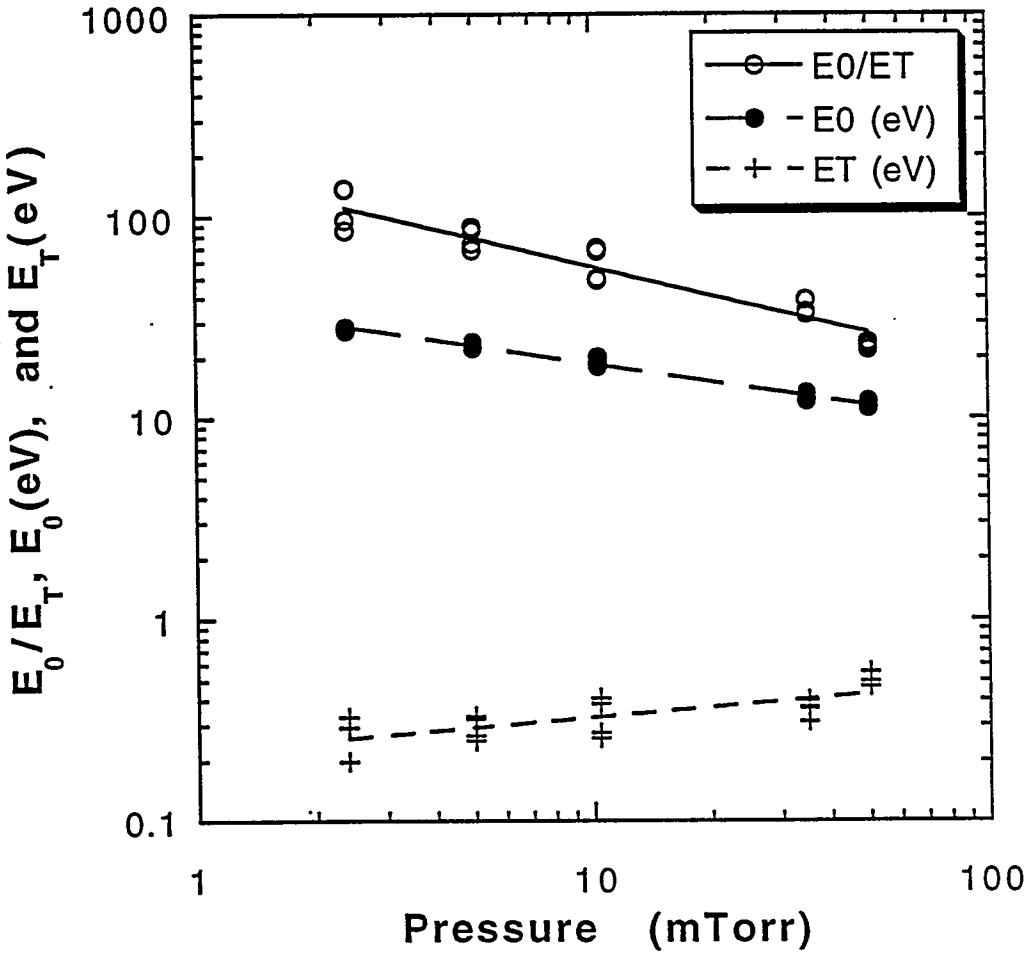

Figure 16. Transverse ion temperatures, directed ion energies and ratio of directed energy to transverse temperature for a number of RF discharges in argon. A 2-micron pinhole was used for these measurements.

(Intentionally left blank)

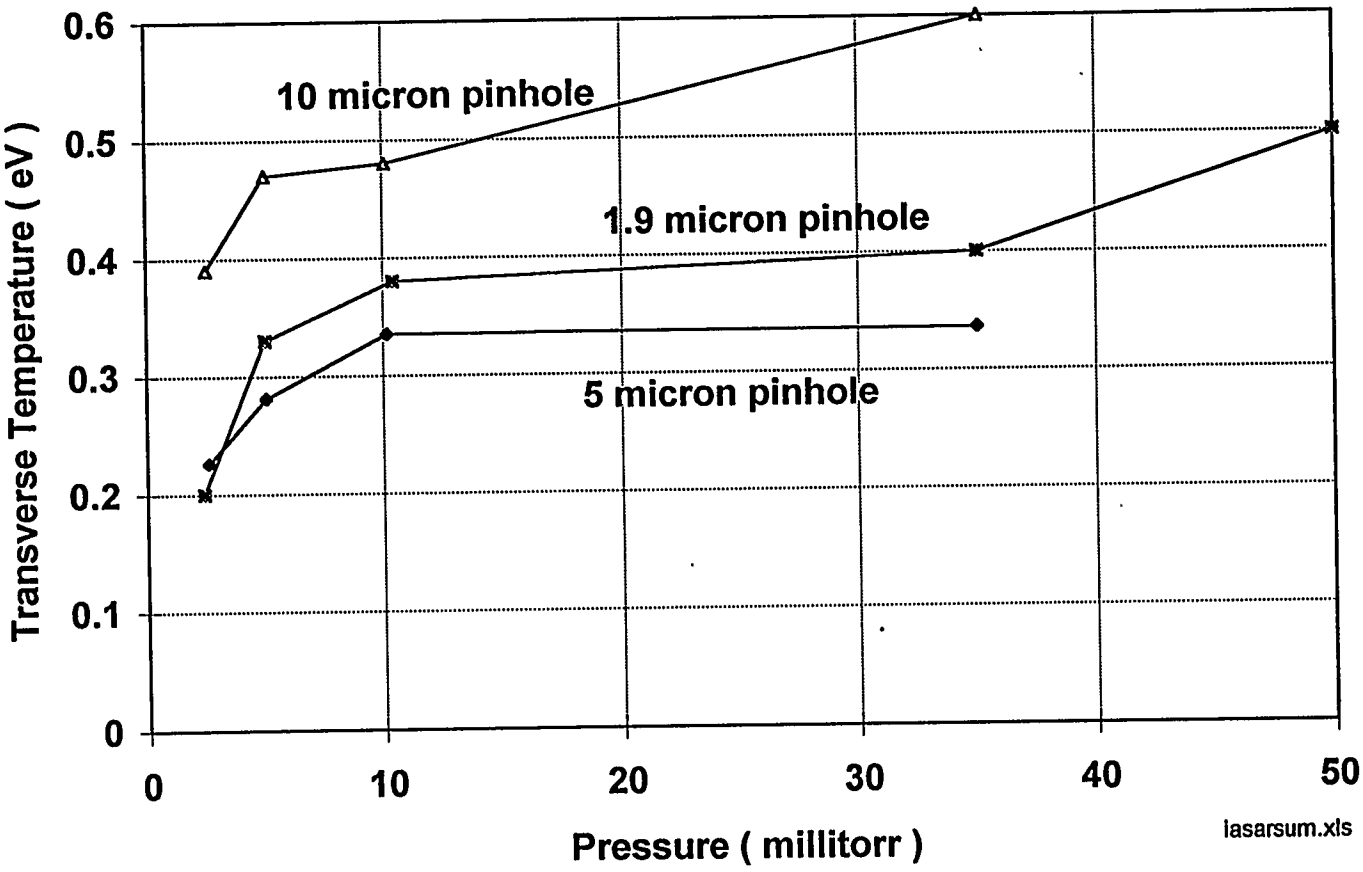

Figure 17. Transverse temperatures measured in argon discharges as a function of the pinhole size used in the experiments. The 5 and 2 micron pinhole data are essentially identical, indicating that with these small pinholes, fringing fields around the pinhole did not significantly affect the angular distribution.

(Intentionally left blank)

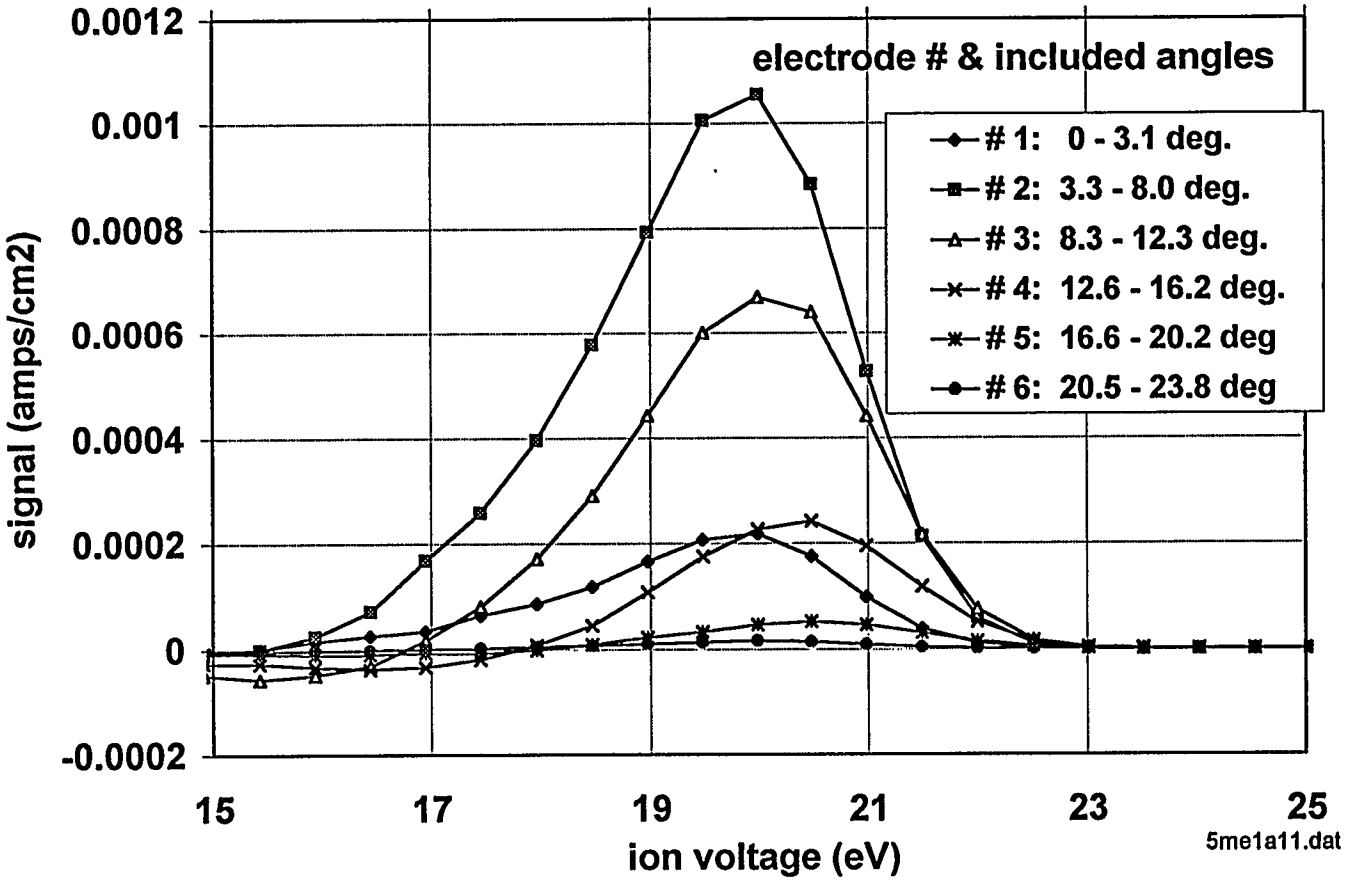

Figure 18. Ion energy distributions in an Ar discharge for ions passing through the pinhole at a number of different angles. This data was taken by measuring ion energy distributions of ions striking individual ring electrodes on the isolated detector. Note that the ion energy distributions are nearly independent of angle.

(Intentionally left blank)

Distribution:

1 H. M. Anderson
Dept. of Chemical & Nuclear Engineering
University of New Mexico
209 Farris Engineering Center
Albuquerque, NM 87131-1341

1 J. L. Cecchi
Dept. of Chemical & Nuclear Engineering
University of New Mexico
209 Farris Engineering Center
Albuquerque, NM, 87131-1341

1 Svetlana Radovanov
Dept of Chemical & Nuclear Engineering
University of New Mexico
209 Farris Center
Albuquerque, NM 87131-1341

1 M. J. Kushner
Dept of Electrical & Computer Engineering
University of Illinois at Urbana-Champaign
1406 West Green St.
Urbana, Illinois, 61801

1 D. B. Graves
Dept of Chemical Engineering
UC Berkley
Berkley, CA, 94720

1 Vikram Singh
Lam Reserach Corporation
4650 Cushing Parkway
Fremont, CA, 94538-6470

1 J. K. Olthoff
Electricity Division
B344 Metrology Bldg, NIST
Gaithersburg, MD, 20899

1 Andrew Labun
Digital Equipment Corporation
77 Reed Road, HLO2/J09
Hudson Mass. 01749-2895

1 Michael J. Hartig
Motorola
Advanced Product R & D Laboratory
3501 Ed Bluestein Blvd.
Austin, Texas 78721

1 H. H. Sawin
Massachusetts Institute of Technology
Rm. 66-505
77 Massachusetts Ave.
Cambridge, Mass 02139

1 Minh S. Le
Massachusetts Institute of Technology
Rm. 66-219
77 Massachusetts Ave.
Cambridge, Mass. 02139

1 Demetre Economou
Dept of Chemical Engineering S 222 D
University of Houston
Houston Texas, 72204

1 Uwe Kortshagen
Dept of Physics
University of Wisconsin - Madison
1150 University Ave.
Madison, Wisconsin 53706

1 George Collins
Dept. of Electrical Engineering
Colorado State University
Fort Collins, Colorado 80523

1 Chunshi Cui
Applied Materials
MS 1125
3320 Scott Boulevard
Santa Clara, California 95094

1	MS:	1423	G. N. Hays, 1128
1		1423	B. P. Aragon, 1128
1		1423	T. W. Hamilton, 1128
1		1423	G. A. Hebner, 1128
1		1423	D. C. Meister, 1128
1		1423	P. A. Miller, 1128
1		1423	M. E. Riley, 1128
8		1423	J. R. Woodworth, 1128
1		9043	E. Meeks, 8745
1		0827	R. T. McGrath, 9114
1		0827	R. B. Campbell, 9114
1		0827	T. J. Bartel, 9114
1		0827	J. E. Johannes, 9114
1		0827	S. J. Choi, 9114
1		0827	R. Veerasinham, 9114
1		9018	Central Tech Files, 8523-2
5		0899	Technical Library, 4414
1		0619	Print Media, 12615
2		0100	Document Processing, 7613-2
36			DOE/OSTI